High-temperature superconducting nanowires for photon detection

R. Arpaia[a,b,c], M. Ejrnaes[b], L. Parlato[b,c], F. Tafuri[b,d], R. Cristiano[b], D. Golubev[e], Roman Sobolewski[f,g], F. Lombardi[a], and G. P. Pepe[b,c]

[a]Quantum Device Physics Laboratory, Department of Microtechnology and Nanoscience, Chalmers University of Technology, S-41296 Göteborg, Sweden

[b]CNR SPIN Institute - Superconductors, Innovative Materials and Devices, UOS–Napoli, I-80100 Napoli, Italy

[c]Dipartimento di Fisica, Università degli Studi di Napoli 'Federico II', I-80125 Napoli, Italy

[d]Dipartimento di Ingegneria Industriale e dell'Informazione, Seconda Università di Napoli, I-81031 Aversa (CE), Italy

[e]Low Temperature Laboratory (OVLL), Aalto University School of Science, P.O. Box 13500, FI-00076 Aalto, Finland

[f]Institute of Electron Technology, PL-02668 Warszawa, Poland

[g]Department of Electrical and Computer Engineering and Laboratory for Laser Energetics, University of Rochester, NY 14627-0231, USA

Email: arpaia@chalmers.se

Abstract

The possible use of high-temperature superconductors (HTS) for realizing superconducting nanowire single-photon detectors is a challenging, but also promising aim, because of their ultrafast electron relaxation times and high operating temperatures. The state-of-the-art, highly homogeneous HTS nanowires with a 50-nm thickness and widths down to 90 nm in a serial-parallel configuration have been fabricated and tested under a 1550-nm wavelength, pulsed laser irradiation. Experimental results presenting both the amplitude and rise times of the photoresponse signals as a function of the normalized detector bias current, measured in the temperature range from 5 K to the critical temperature, are discussed. The presence of two, distinct regimes in the photoresponse temperature dependence is clearly evidenced, indicating that there are two different response mechanisms responsible for the HTS photoresponse mechanisms.

1. Introduction

The first operational superconducting nanowire single-photon detector (SNSPD) was demonstrated in 2001 by Gol'tsman *et al*. [1]. Currently, developing high-performance SNSPDs is an intensively investigated topic within both the quantum optics and superconducting electronics communities [2]. The SNSPD is the first photon counter to achieve <100-ps timing jitter and up to hundreds of MHz counting rates, presently exceeding the best results for any other SPD technologies. The SNSPD operation is based on superconducting-to-normal transition of a nanostripe, typically fabricated as a meander covering up to 10 × 10 μm^2. To scale-up SNSPDs toward larger areas, as is required in several applications, one needs more complex, e.g., array-type configurations. Additionally, all present SNSPDs are operated in the ultralow temperature range of 1.7 to 5 K because they are based on conventional, metallic superconductors like NbN, NbTiN, Nb, or WSi.

The liquid-helium cooling requirement and the relatively small active area are the main disadvantages of conventional SNSPDs, limiting their applications especially at the near-infrared (NIR) wavelengths (~1 to 3 μm), where, otherwise, they would have no serious competitors. Among potential NIR applications are interplanetary optical communications; quantum optics experiments, including quantum key distribution schemes [3], and intensity correlation measurements [4,5], as well as laser ranging and telecommunication [6], optical time-domain reflectometry, fluorescence-correlation spectroscopy [7], fluorescence lifetime measurements [8], and, finally, astronomical observations of photon "starved" sources [9].

SNSPD development would not be possible without the progress made over the past decade in nanotechnology and, in particular, in nanopatterning of superconducting

thin films. The achieved sensitivity of the ~1-eV energy released by absorption of a single NIR photon is obtained only because of a nanometer-size cross-sectional area of the nanostripe, which is the sensitive element of the SNSPD. The challenge in fabricating high-quantum-efficiency (QE) SNSPDs is obtaining high uniformity both in the width and thickness over the nanostripe length, which in meander structures can be as high as 0.5 mm. This is typically accomplished by using electron-beam-lithography (EBL) technology. The latest is most challenging in very large active area (40 × 40-μm^2) SNSPDs with so-called *parallel* architectures, like those recently developed to increase the signal-to-noise ratio, the speed, and the photon-counting capabilities [10,11].

Choosing the most-suitable superconducting material for the SNSPD is another important issue. Conditions such as a short coherence length, intrinsic fast-quasiparticle recombination time, and, simultaneously, the highest possible transition temperature must be satisfied [1]. Obviously, a high-temperature superconductor (HTS), such as $YBa_2Cu_3O_{7-x}$ (YBCO), meets all these requirements and, therefore, is a good candidate for advanced SNSPDs. Unfortunately, several drawbacks in the YBCO state-of-the-art technology make realizing YBCO-based SNSPDs a very challenging task. Furthermore, superconductivity of HTS materials and, in particular, in HTS nanostructures, is quite different from the conventional/metallic case. However, this aspect also creates an opportunity since the HTS nanostripes can open new scenarios for some intrinsic mechanisms involved in forming the photoresponse signal. The latter can shed new light on the microscopic mechanism of photon detection in superconducting nanostructures.

Serious degradation of the superconducting properties typically occurs in YBCO films when their thickness and/or width approach the nanometer scale and is caused by

the edge damage related to a nanopatterning procedure, resulting oxygen out-diffusion [12–16]. This is most evident when the HTS film thickness is reduced to 5 to 10 nm–the thickness typically used in the case of metallic SNSPD meanders. Another concern is the response mode of YBCO nanostripes: while metallic SNSPDs are classified as quantum (nonequilibrium) detectors with single-photon sensitivity, it is extremely difficult to fabricate HTS nanowires with such cross-sectional areas that guarantee a non-bolometric photoresponse and, consequently, single-photon sensitivity. Finally, a typical current-voltage (I–V) characteristics of an YBCO nanostripe exhibits a gradual, rather than a sharp superconducting-to-resistive state transition, because of the presence of a flux–flow regime, where a resistive state appears, but the superconductivity is still present in the sample [17].

This latter aspect and the ultrashort recovery time of the superconducting state in HTS materials lead to some peculiar aspects in their photoresponse, quite different from the conventional superconductor case. HTS nanostripes are extremely two-dimensional (2-D) superconductors with respect to both the coherence length and the London penetration depth. Thus, such microscopic mechanisms of photon detection like quantum-mechanical or thermally activated phase-slip centers (PSCs), unbinding of vortex–antivortex pairs (VAPs), quantum-mechanical tunneling of vortices, or thermal excitation of single vortices across the stripe-edge barrier and their subsequent dissipative movement across the stripe width, can all play a very significant role.

Ultrathin films of YBCO have already been realized; therefore, we report here only the most recent literature results. In [18], YBCO films ranging from 80 nm down to 10 nm were deposited on a sapphire substrate with a $CeO_2/PrBa_2Cu_3O_{7-x}$ buffer bilayer and with a $PrBa_2Cu_3O_{7-x}$ overlayer deposited on top for YBCO film protection.

The 10-nm-thick film, which corresponds to only eight unit cells, reached T_c = 79 K. These films were used to realize 2-μm-long, 4.5-μm-wide superconducting microbridges. In [19], 10-nm-thick films grown on (100) MgO substrates were used to realize 100-nm × 100-nm constrictions for hot-electron bolometers. The only attempt to realize SNSPD meanders with long nanostripes was reported in [20], where a 12-nm-thick YBCO film was patterned in an attempt to realize a 430-μm-long, 1-μm-wide nanowire. Using the same process, the authors were also able to fabricate 500-nm wide, 15-μm-long single stripes; however, no photoresponse was observed.

It should be mentioned that YBCO bridges with a thickness in the range of 40 to 300 nm, a length of 50 to 200 μm, and a width 10 to 100 μm, as well as meander patterns, were studied under a pulsed optical excitation and the photoresponse was observed at temperatures in the close vicinity of the transition region to the normal state [21]. A bolometric component in the optical response was observed and attributed to additional flux creep and flux motion caused by the absorption of optical photons that caused additional dissipation, equivalent to the increase in the bridge resistance. This component disappeared when the temperature decreased well below T_c.

In this work, we present YBCO-based nanowires and study their photoresponse under pulsed optical illumination at the 1550-nm wavelength in a temperature range from 4 K up to T_c. Our experimental results should be considered as a first step toward full understanding of a complex physical picture of the HTS nanostripe photoresponse.

2. Optical Photoresponse of a Superconducting Nanostripe

Although details of a microscopic mechanism of photon detection in SNSPDs are still under debate, a supercurrent-assisted, hotspot formation is considered the main ingredient of the *normal-core hotspot model* that was introduced in the original papers reporting the SNSPD photodetection [1,22–25]. When the superconducting nanostripe, biased close to its critical current I_c, is hit by a photon, the energy of the absorbed photon E_{ph} is usually much larger than the superconducting energy gap Δ (for optical photons $E_{ph} > 1$ eV, while for metallic materials, typically, $\Delta \approx 1$ to 2 meV) and, as a consequence, a cascade of quasiparticle (QP) relaxation leads to a region of depressed superconductivity around the absorption site; i.e., the so-called, hotspot. Since the nanowire is biased close to I_c, the hotspot can further expand thermally, resulting in a normal region (destroyed superconductivity) across the stripe around the absorption site. When the whole cross-sectional area of the nanowire becomes normal, the bias current is deviated onto the external load R_L of the read-out circuit, generating the output-voltage pulse V on nanosecond time scales. By measuring the voltage pulses, the radiation can be detected and photons counted.

Superconducting and, simultaneously, light absorbing properties of the SNSPD material play an important role in determining the hotspot size and resulting region of destroyed superconductivity after photon excitation. In general, the increase of the incident E_{ph} results in the increased number of QPs generated in the avalanche and results in a larger hotspot. Therefore, for a superconductor with a small Δ, as compared to E_{ph}, correspondingly lower photon energy is needed to create a sufficient amount of

QPs, making such material more sensitive for longer-wavelength photons. In addition, materials with low density of states are preferable, because a smaller number of Cooper pairs must be broken to create the normal-state zone. Independently, the stripe cross section has to be minimized, since the decrease of the cross section leads to the lower the photon energy required to create the normal-conducting region triggering the count pulse. Once the energy deposited by the photon dissipates from the normal-state region and the cooling power is sufficient to counter the heat dissipation of the bias current, the SNSPD falls back to its initial superconducting state. Intrinsically, the time constant for this process is the electron-phonon relaxation time τ_{e-ph}, but in most common meander-type SNSPDs, it is actually limited by the kinetic inductance of the superconducting meander and the external electrical circuitry, and is in the range of nanoseconds.

It remains an open question whether magnetic vortices play any role in the superconducting-nanostripe-detection mechanism. There are two variations of the vortex-based models. The first is an extension of the normal-state model, where a single VAP forms at the point where the photon is absorbed. In the second, local weakening of the superconductivity lowers the energy barrier for a vortex crossing [26–29]. In both scenarios, the role of the incident photon in the detection process is to locally depress superconductivity. Subsequently, thermally activated fluctuations occur, such as the de-pairing of a VAP [30] or the single-vortex crossing. These fluctuations must overcome an energy barrier $E(\Delta,I_b)$ [29]. Expressions for such energy barriers typically contain a gap-dependent energy scale and a current-dependent geometric factor [31]. An extensive study of various current-induced fluctuation phenomena in superconducting nanoscaled meander structures has been conducted by Bartolf *et al*. [32], to decide on the mechanism responsible for NIR photon detection. Once the vortex is introduced into

the nanostripe, the Lorentz force will act on it as a result of the bias current and it will start to move across the stripe. Since the energy dissipated in this case is similar to the energy of an optical photon, this will lead to a count event. If an NIR photon is absorbed, Δ is locally suppressed and, consequently, the potential barrier will be reduced by ΔU. The probability P for a vortex to be excited over the barrier is proportional to $\exp(-U/k_BT)$ [33,34]. It must be stressed that, depending on the thermal activation energy, this process can also happen even without photon absorption and such an effect is considered a dark-count event. Finally, recently, PSCs have also been considered as switching mechanisms for the bias-current values very close to the de-pairing I_c limit in the case of nanowires with bends [35].

In YBCO the two main QP interaction times are the subpicosecond thermalization time and picosecond τ_{e-ph} range, as was measured by the electro-optical sampling technique [36]. Simultaneously, the specific heat capacity of the phonons C_{ph} is much larger than the electron-specific heat capacity C_e ($C_{ph}/C_e = 38$) [36]. Therefore, on a femtosecond time scale, the hot electron and phonon subsystems are thermally decoupled, and the energy backflow from the phonon to the electron system can be neglected. Furthermore, YBCO is a layered superconductor, which may imply that forming the hotspot in such a material could have peculiarities, resulting, for instance, in the possibility that the constraint on the stripe thickness could be relaxed. The dynamics of vortices in YBCO is also peculiar; therefore, vortices could play a different role than in conventional 2-D superconducting stripes. Finally, the presence of PSCs or even so-called PS lines cannot be ruled out as an additional photoresponse mechanism in HTS nanowires. All these features make the investigation of YBCO SNSPDs a very interesting topic.

3. YBCO Nanowires: Fabrication Technology

The first ingredient for realizing SNSPDs is the technology required to fabricate YBCO stripes with the desired thickness, width, and length. Nanopatterning techniques are very well established for LTS materials; thence few nanometers thick and sub-micrometer wide, millimeter-long nanowires can be routinely achieved without observing any severe degradation of the superconducting properties. For HTS materials, realization of nanostripes with sub-micrometer cross-section dimensions and highly homogeneous superconducting properties is still extremely challenging.

In this work, we fabricated 50-nm-thick YBCO nanostripes on LAO substrates. Their widths were in the range of 90 to 500 nm, while the lengths varied up to 10 μm, increasing proportionally to a given sample width. The distance between wires was fixed and equal to 500 nm. We were able to achieve devices (see, e.g., in Fig. 1) covering areas up to 30 × 10 μm^2, with a filling factor of 50%. To minimize current crowding effects [37,38], which could be a further source of reduction of the critical current densities (J_c's) in our nanostripes, the edges between the wires and the wider electrodes were designed with a rounded shape, as shown in Fig. 1(b).

As reported in [39], our basic 50-nm-thick YBCO films were deposited using a pulsed-laser-deposition system on (001) LAO substrates at an O_2 pressure of 0.6 mbar and deposition temperature of 800°C. The surface roughness of the resulting films was only 2 nm and they showed excellent structural and transport properties with about 0.3° full width at half maximum rocking curves of the (005) reflection, and a very sharp superconducting transition with $T_c \approx 89$ K. To protect the YBCO film from any damages occurring during the patterning steps, a cap layer of a 50-nm-thick Au film was deposited by e-beam evaporation, as reported in [38,40]. The Au layer was

removed using Ar etching before the photoresponse measurements. Depending on the nanowire width, their T_c varied from 80 to 85 K (500-nm-wide stripe).

Considering that our samples are intended to operate as photon detectors, we need large areas to maximize the detection efficiency of the devices. In particular, we have chosen the parallel-wire configuration, consisting of a serial connection of blocks (7, 9, 11, and 13), each formed by three nanowires in parallel (see Fig. 1). As a consequence of this geometry, we expect the photoresponse signal to be enhanced in amplitude since it is proportional to the current corresponding to the sum of currents in all our parallel nanowires. Moreover, a parallel connection of nanostripes reduces the total kinetic inductance of a given structure, resulting in a faster signal response. The performance of such device, in terms of signal amplitude, is related to the capability to fabricate stripes with very high critical current densities, together with a high degree of homogeneity of the stripes.

4. Transport and Photoresponse Measurements

The nanowire structures described above were first characterized in terms of the I–V curves used to extract the J_c's before and after removing the Au cap layer. With the Au present, the YBCO nanowire-transport properties followed the same behavior as already observed in previous publications [38,40], with the J_c as high as ~10^7 A/cm^2, independent of the wire width. After the Au cap was completely etched, the J_c values were reduced about one order of magnitude for all widths.

In the next step, the temperature dependence of our nanowire devices was investigated. Figure 2 shows the dependence of I_c normalized to I_c (5 K) on normalized T/T_c for a naked, 500-nm-wide YBCO nanostripe. We notice that our experimental data

points can be quite well fitted (solid line in Fig. 2) by the Bardeen formula, commonly used to describe metallic superconducting nanowires in the dirty limit [42]:

$$I_c(T) \propto \left[1-\left(\frac{T}{T_c}\right)^2\right]^{3/2}. \quad (1)$$

The deviation of the $I_c(T)$ data from Eq. (1) observed at high temperatures is, most likely, due to some damage induced by the nanostripe patterning and, subsequent, etching of the Au cap layer [40].

Photoresponse experiments have been carried out by mounting test devices in a liquid-helium, continuous-flow cryostat having an optical access. The nanowires were illuminated by 1550-nm-wavelength optical laser pulses. The laser pulses had rise and fall times of 3 ns, a duration between 10 and 500 ns, and a nominal intensity of ~50 nW/μm^2. Figure 3 shows voltage photoresponse signals [red dots in insets (a), (b), and (c)] plotted as a function of time for a 500-nm-wide YBCO nanowire. The insets are overlaid on top of the I–V curve measured at the experiment 8-K temperature, in order to indicate different biasing regimes in the: (a) below I_c, (b) very close to I_c, and (c) above I_c on the resistive branch. In each inset, the photoresponse signals are overlaid with the inverse of laser pulses used to illuminate the devices (blue lines). We observe that the photoresponse appears when the device is biased slightly below I_c, reaches maximum roughly at $I_b \approx I_c$ [Fig. 3(b)], and afterward, continues in the resistive state [Fig. 3(c)]. However, above I_c, the signal amplitude decreases with the I_b increase and either vanishes completely or reaches a low-level saturation value (few ΔV) at $I_b >> I_c$.

On the other hand, when our nanostripe is in the fully superconducting state, i.e., biased far below I_c, no measureable photoresponse is detected [Fig. 3(a)].

The behavior observed in Fig. 3 is markedly different than that routinely observed in conventional SNSPDs. In our YBCO-based nanowires, the measured resistive branch of the I–V curve represents an intermediate or mixed state, where both superconducting and normal states coexist. The high value of the thermal conductivity in the YBCO case (~2 Wm^{-1} K^{-1}) prevents self-heating effects that could bring the entire device into the normal state above I_c. On the other hand, this is what always happens in NbN nanowires, where thermal conductivity is almost two orders of magnitude lower. In the metallic nanowire case, I–V curves are highly hysteretic and a very large voltage switch occurs just above I_c, bringing the structure into the normal state. In agreement with the hotspot detection model, a metallic SNSPD after photon absorption exhibits normal resistance that is much larger than the external load of the readout circuit and the total I_b is redirected into the readout line. As a result, the output signal is proportional to I_bR_L and no trace of photoresponse is visible when $I_b > I_c$. In the case of YBCO nanowires, the hotspot is unable to drive a whole nanowire into the normal state, but generates only an intermediate state, where most likely fluxon dynamics plays a fundamental role.

We have also investigated the role of temperature on the photoresponse of devices with different stripes widths (up to 500 nm). Voltage pulses unambiguously corresponding to the incident laser pulses have been detected from 5 K up to T_c. In Fig. 4, we plot the nanowire maximum photoresponse signal measured at $I_b \approx I_c$ as a function of the reduced temperature T/T_c. We observe that the signal is a monotonically

decreasing function of temperature. The decrease rate is much more pronounced at low temperatures, while at T slightly below T_c the photoresponse is almost constant. Very similar behavior was observed for all our samples with the widths up to 500 nm.

Finally, we combine our photoresponse signal bias and temperature studies and we present them in Fig. 5. In Fig. 5(a), we show a family of normalized amplitudes of the photoresponse signals versus normalized biasing I_b/I_c for a 500-nm-wide YBCO device, collected at different temperatures. We observe clear evidence of the presence of two different regimes separated by the threshold temperature close to 50 K. A very similar behavior was found in the dependence of the photoresponse signal rise times (i.e., time differences corresponding to 10% and 90% of the full amplitude) versus I_b/I_c, measured at different temperatures and presented in Fig. 5(b). The rise-time values are about one order of magnitude longer at temperatures above 50 K, as compared to the ones measured at low temperatures (<20 K). In addition, there is no dependence on I_b in the high-temperature region.

Analyzing the above data, we suspect that heating is a significant component of the high-temperature photoresponse signal. A similar behavior was observed for a Josephson junction in presence of thermal noise [43]. Within this context, a non-bolometric component is likely to be present at low temperatures (below ~50 K), where higher-amplitude photoresponse signals with faster rise times are recorded.

More experiments at reduced cross sections of the nanowires, in particular with lower thicknesses, are needed in order to better understand the physics behind the photoresponse signal formation in YBCO nanostructures. We stress that especially for ultrathin (~10 nm thick) nanowires the presence of a cap layer is crucial to assure the homogeneity of the crystalline structure and the oxidization level of YBCO. In the

future, different materials, like $La_{0.7}Sr_{0.3}Mn_3$ (LSMO) or carbon, will be considered as possible cap layers in our research. LSMO as a magnetic material with the Curie temperature well above room temperature is an especially interesting cap layer, since it plays an active role in the photon-detection process [44].

5. Conclusions

We fabricated and experimentally tested superconducting YBCO nanowires with cross sections down to 50 × 90 nm^2 that were highly homogeneous and exhibited excellent structural and transport properties. As a device configuration, we have chosen a serial-parallel nanostripe geometry, consisting of a serial connection of blocks (7, 9, 11, and 13), each formed by three nanowires in parallel with areas up to 30 × 10 μm^2 and a fill factor of 50%. In this geometry the photoresponse signal is proportional to the current corresponding to the sum of currents in all our parallel nanowires, while a parallel connection of nanostripes reduces the total kinetic inductance of a given structure, resulting in a faster signal response. Photoresponse signals were clearly observed under optical laser pulses at a 1550-nm-wavelength illumination at temperatures from 5 K up to T_c and were investigated for different nanowires as a function of the bias current. The presence of two, distinct regimes in the photoresponse temperature dependence was clearly evidenced, indicating the two, distinct response mechanisms responsible for the HTS photoresponse mechanisms. The use of a protective overlayer, transparent to our optical irradiation (contrary to Au), appears to be a natural future route to improve both the optical and electrical properties of YBCO nanostructures and, simultaneously, preserve bulk-like values of both T_c and J_c. The

latter will be the direction of our future investigations, hopefully leading to practical HTS single-photon detectors operating at elevated temperatures.

Acknowledgment

The work was partially supported by the Swedish Research Council (VR) and the Knut and Alice Wallengerg Foundation (Göteborg), and by EU under the MAMA project (Napoli) and the European Regional Development Fund through the Innovative Economy "MIME" grant POIG.01.01.02-00-108/09 (Warsaw). Additionally, we acknowledge the EU COST Action MP1201.

References

[1] G.N. Gol'tsman, O. Okunev, G. Chulkova, A. Lipatov, A. Semenov, K. Smirnov, B. Voronov, A. Dzardanov, C. Williams, R. Sobolewski, Picosecond superconducting single-photon optical detector, Appl. Phys. Lett. 79 (2001) 705–707.

[2] C.M. Natarajan, M.G. Tanner, R.H. Hadfield, Superconducting nanowire single-photon detectors: Physics and applications, Supercond. Sci. Technol. 25 (2012) 063001 and the references therein.

[3] H. Takesue, S.W. Nam, Q. Zhang, R.H. Hadfield, T. Honjo, K. Tamaki, Y. Yamamoto, Quantum key distribution over a 40-db channel loss using superconducting single-photon detectors, Nature Photon. 1 (2007) 343–348.

[4] R.H. Hadfield, M.J. Stevens, S.S. Gruber, A.J. Miller, R.E. Schwall, R.P. Mirin, S.W. Nam, Single photon source characterization with a superconducting single photon detector, Opt. Express 13 (2005) 10846–10853.

[5] M. Halder, A. Beveratos, N. Gisin, V. Scarani, C. Simon, H. Zbinden, Entangling independent photons by time measurement, Nature Phys. 3 (2007) 692–695.

[6] R.E. Warburton, A. McCarthy, A.M. Wallace, S. Hernandez-Marin, R.H. Hadfield, S.W. Nam, G.S. Buller, Subcentimeter depth resolution using a single-photon counting time-of-flight laser ranging system at 1550 nm wavelength, Opt. Lett. 32 (2007) 2266–2268.

[7] S.T. Hess, S. Huang, A.A. Heikal, W.W. Webb, Biological and chemical applications of fluorescence correlation spectroscopy: A review, Biochemistry 41 (2001) 697–705.

[8] W. Becker, A. Bergmann, M.A. Hink, K. König, K. Benndorf, C. Biskup, Fluorescence lifetime imaging by time-correlated single-photon counting, Microsc. Res. Tech. 63 (2004) 58–66.

[9] J.C. Mather, Super photon counters, Nature 401 (1999) 654–655.

[10] F. Mattioli, M. Ejrnaes, A. Gaggero, A. Casaburi, R. Cristiano, S. Pagano, R. Leoni, Large area single photon detectors based on parallel configuration NbN nanowires, J. Vac. Sci. Technol. B 30 (2012) 031204.

[11] F. Marsili, F. Najafi, E. Dauler, F. Bellei, X. Hu, M. Csete, R.J. Molnar, K.K. Berggren, Single-photon detectors based on ultranarrow superconducting nanowires, Nano Lett. 11 (2011) 2048–2053.

[12] P. Larsson, B. Nilsson, Z.G. Ivanov, Fabrication and transport measurements of $YBa_2Cu_3O_{7-x}$ nanostructures, J. Vac. Sci. Technol. B 18 (2000) 25–31.

[13] H. Assink, A.J.M. Harg, C.M. Schep, N.Y. Chen, D. Marel, P. Hadley, E.W.J.M. Drift, J.E. Mooij, Critical currents in submicron $YBa_2Cu_2O_7$ lines, IEEE Trans. Appl. Supercond. 3 (1993) 2983–2985.

[14] S. Nawaz, T. Bauch, F. Lombardi, Transport properties of YBCO nanowires, IEEE Trans. Appl. Supercond. 21 (2011) 164–167.

[15] F. Tafuri, D. Massarotti, L. Galletti, D. Stornaiuolo, D. Montemurro, L. Longobardi, P. Lucignano, G. Rotoli, G. Pepe, A. Tagliacozzo, F. Lombardi, Recent achievements on the physics of high-T superconductor Josephson junctions: Background, perspectives and inspiration, J. Supercond. Nov. Magn. 26 (2013) 21–41.

[16] D. Gustafsson, D. Golubev, M. Fogelström, T. Claeson, S. Kubatkin, T. Bauch, F. Lombardi, Fully gapped superconductivity, Nature Nanotechnol. 8 (2013) 25–30.

[17] D. Golubev, F. Lombardi, T. Bauch, "Effect of heating on critical current of YBCO nanowires", Physica C (2014), doi: http://dx.doi.org/10.1016/j.physc.2014.06.013

[18] P. Probst, A. Semenov, M. Ries, A. Hoehl, P. Rieger, A. Scheuring, V. Judin, S. Wünsch, K. Il'in, N. Smale, Y.L. Mathis, R. Müller, G. Ulm, G. Wüstefeld, H.W. Hübers, J. Hänisch, B. Holzapfel, M. Siegel, A.S. Müller, Nonthermal response of $YBa_2Cu_3O_{7-x}$ thin films to picosecond THz pulses, Phys. Rev. B 85 (2012) 174511.

[19] R.G. Ladret, A.F. Degardin, A.J. Kreisler, Nanopatterning and hot spot modeling of YBCO ultrathin film constrictions for THz mixers, IEEE Trans. Appl. Supercond. 23 (2013) 2300305.

[20] N. Curtz, E. Koller, H. Zbinden, M. Decroux, L. Antognazza, Ø. Fischer, N. Gisin, Patterning of ultrathin YBCO nanowires using a new focused-ion-beam process, Supercond. Sci. Technol. 23 (2010) 045015.

[21] A. Frenkel, M.A. Saifi, T. Venkatesan, P. England, X.D. Wu, A. Inam, Optical response of nongranular high-T_c $Y_1Ba_2Cu_3O_{7-x}$ superconducting thin films, J. Appl. Phys. 67 (1990) 3054–3068.

[22] J. Zhang, W. Słysz, A. Pearlman, A. Verevkin, R. Sobolewski, O. Okunev, G. Chulkova, G.N. Gol'tsman, Time delay of resistive-state formation in superconducting stripes excited by single optical photons, Phys. Rev. B 67 (2003) 132508.

[23] R. Sobolewski, A. Verevkin, G. N. Gol'tsman, A. Lipatov, and K. Wilsher, Ultrafast Superconducting Single-Photon Optical Detectors and Their Applications, IEEE Trans. Appl. Supercon. 13 (2003) 1151–1157.

[24] A. D. Semenov, G. N. Gol'tsman, A. A. Korneev, Quantum detection by current carrying superconducting film, Physica C 351 (2001) 349–356.

[25] A. Engel, K. Inderbitzin, A. Schilling, R. Lusche, A. Semenov, H.-W. Hübers, D. Henrich, M. Hofherr, K. Il'in, M. Siegel, Temperature-dependence of detection efficiency in NbN and TaN SNSPD, IEEE Trans. Appl. Supercond. 23 (2013) 2300505.

[26] A. Semenov, A. Engel, H.W. Hübers, K. Il'in, M. Siegel, Spectral cut-off in the efficiency of the resistive state formation caused by absorption of a single-photon in current-carrying superconducting nano-strips, Eur. Phys. J. B 47 (2005) 495–501.

[27] A. Gurevich, V.M. Vinokur, Comment on 'vortex-assisted photon counts and their magnetic field dependence in single-photon superconducting detectors' Phys. Rev. B 86 (2012) 026501.

[28] A. Gurevich, V.M. Vinokur, Size effects in the nonlinear resistance and flux creep in a virtual Berezinskii-Kosterlitz-Thouless state of superconducting films, Phys. Rev. Lett. 100 (2008) 227007.

[29] L.N. Bulaevskii, M.J. Graf, C.D. Batista, V.G. Kogan, Vortex-induced dissipation in narrow current-biased thin-film superconducting strips, Phys. Rev. B 83 (2011) 144526.

[30] A.D. Semenov, P. Haas, H.-W. Hübers, K. Ilin, M. Siegel, A. Kirste, T. Schurig, A. Engel, Vortex-based single-photon response in nanostructured superconducting detectors, Physica C 468 (2008) 627–630.

[31] M. Hofherr, D. Rall, K. Ilin, M. Siegel, A. Semenov, H.-W. Hübers, N.A. Gippius, Intrinsic detection efficiency of superconducting nanowire single-photon detectors with different thicknesses, J. Appl. Phys. 108 (2010) 014507.

[32] H. Bartolf, A. Engel, A. Schilling, K. Il'in, M. Siegel, H.W. Hübers, A. Semenov, Current-assisted thermally activated flux liberation in ultrathin nanopatterned NbN superconducting meander structures, Phys. Rev. B 81 (2010) 024502.

[33] A. Engel, A.D. Semenov, H.-W. Hübers, K. Il'in, M. Siegel, Fluctuation effects in superconducting nanostrips, Physica C 444 (2006) 12–18.

[34] F. Tafuri, J. R. Kirtley, D. Born, D. Stornaiuolo, P. G. Medaglia, P. Orgiani, G. Balestrino, V. G. Kogan, Dissipation in ultra-thin current-carrying superconducting bridges; evidence for quantum tunneling of pearl vortices, Europhys. Lett. 73 (2006) 948–954.

[35] D.Y. Vodolazov, Saddle point states in two-dimensional superconducting films biased near the depairing current, Phys. Rev. B 85 (2012) 174507.

[36] M. Lindgren, M. Currie, C. Williams, T.Y. Hsiang, P.M. Fauchet, R. Sobolewski, S.H. Moffat, R.A. Hughes, J.S. Preston, F.A. Hegmann, Intrinsic picosecond response times of Y-Ba-Cu-O superconducting photodetectors, Appl. Phys. Lett. 74 (1999) 853–855.

[37] J. R. Clem and K. K. Berggren, Phys. Rev. B. 84, (2011) 174510.

[38] S. Nawaz, R. Arpaia, F. Lombardi, T. Bauch, Phys. Rev. Lett. 110 (2013) 167004.

[39] R. Arpaia, M. Ejrnaes, L. Parlato, R. Cristiano, M. Arzeo, T. Bauch, S. Nawaz, F. Tafuri, G. P. Pepe, F. Lombardi, Highly homogeneous YBCO/LSMO nanowires for photoresponse experiments, Supercond. Sci. Technol. 27 (2014) 044027.

[40] S. Nawaz, R. Arpaia, T. Bauch, F. Lombardi, Approaching the theoretical depairing current in $YBa_2Cu_3O_{7-x}$ nanowires, Physica C 495 (2013) 33–38.

[41] R. Arpaia, S. Nawaz, F. Lombardi, T. Bauch, Improved nanopatterning for YBCO nanowires approaching the depairing current, IEEE Trans. Appl. Supercond. 23 (2013) 1101505.

[42] J. Bardeen, Critical fields and currents in superconductors, Rev. Mod. Phys. 34 (1962) 667–681.

[43] V. Ambegaokar and B.I. Halperin, Phys. Rev. Lett. 22, (1969) 1364.

[44] L. Parlato, R. Arpaia, C. De Lisio, F. Miletto Granozio, G.P. Pepe, P. Perna, V. Pagliarulo, C. Bonavolonta, M. Radovic, Y. Wang, R. Sobolewski, and U. Scotti di Uccio, Ultrafast electron relaxation in all-oxide $YBa_2Cu_3O_7/La_{0.7}Sr_{0.3}MnO_3$ proximitized bilayers by time-resolved spectroscopy, Phys. Rev B 87, (2013) 134514.

Figure Captions:

Fig. 1. (a) Micrograph of a device formed by serial connections of 300-nm-wide parallel YBCO nanowires; (b) An AFM scan of several 130-nm-wide YBCO nanowires. The blunt corners between the wires and the wider electrodes avoid the reduction of the critical current caused by the current crowding effect.

Fig. 2. Normalized critical current values measured in the whole range of temperatures for a 500-nm-wide pure YBCO device (red dots). The experimental data are fitted by the Bardeen expression [42].

Fig. 3. I-V characteristics measured at T = 8 K for a device consisting of of 130-nm-wide YBCO nanowires. The three insets show the time-resolved photoresponse signal (red circles) measured at three different bias currents, corresponding to different regimes on the I-V: (a) the superconducting regime (I_b/I_c = 0.23); (b) the critical regime (I_b/I_c = 0.99); and (c) the resistive/intermediate state regime (I_b/I_c = 1.36). The blue lines correspond to the inverse of pulses used to illuminate the devices.

Fig. 4. The maximum photoresponse signal measured near I_c as a function of the normalized temperature for a 130-nm-wide device. The solid line is used only to guide the eye.

Fig. 5. (a) Normalized photoresponse amplitudes and (b) rise times versus the normalized bias current, collected at several different temperatures for a 500-nm-wide device.

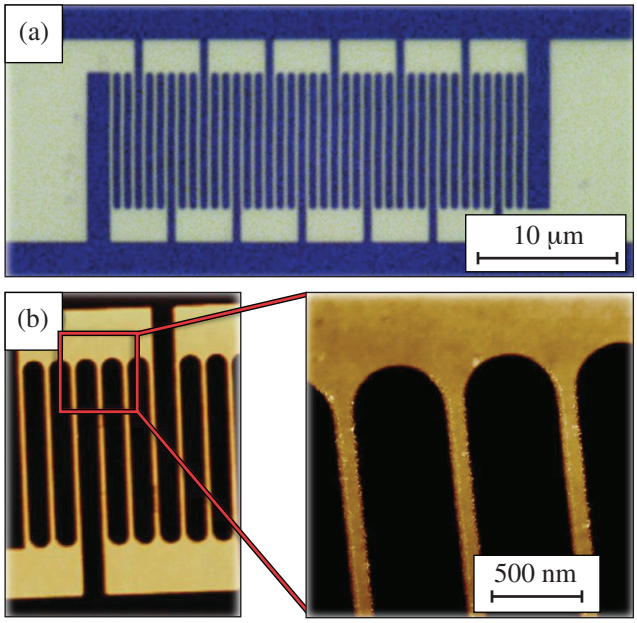

Figure 1

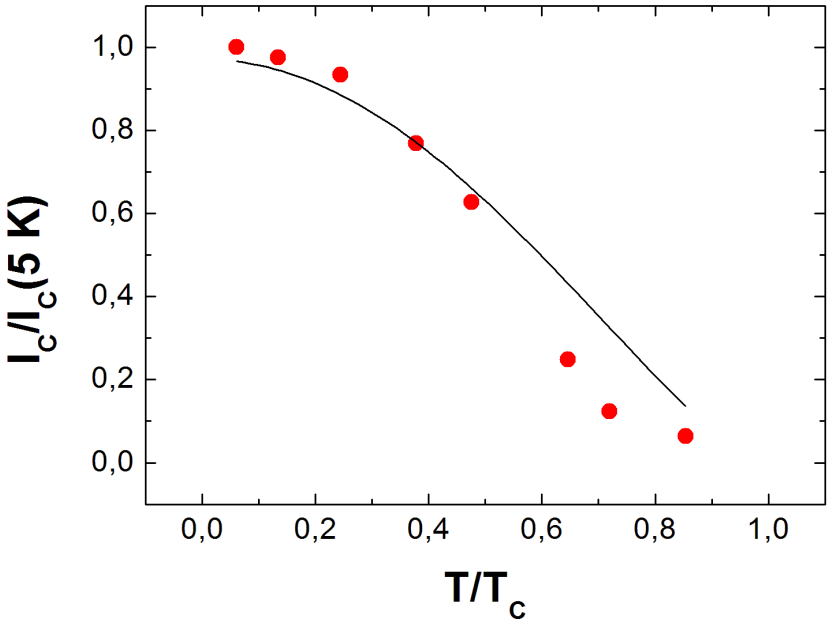

Figure 2

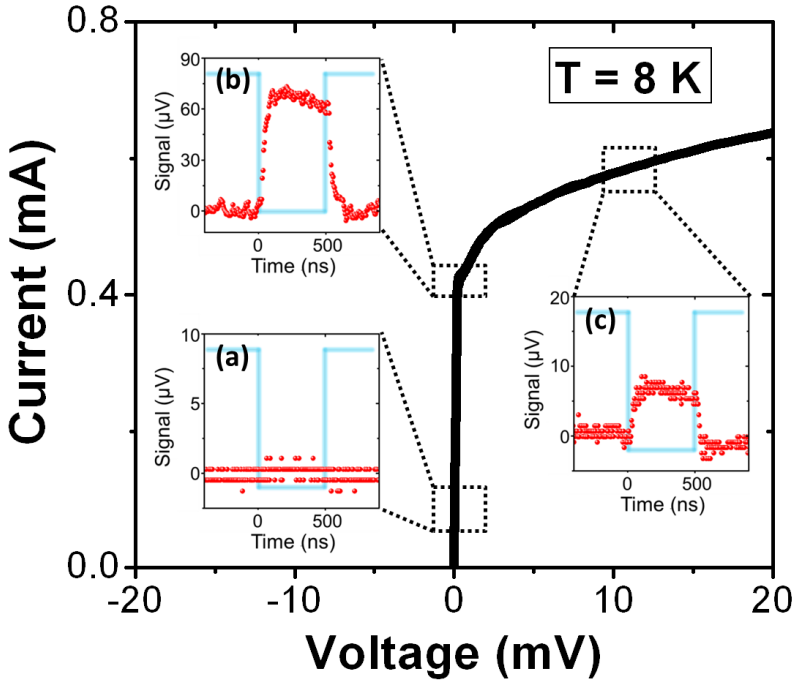
T = 8 K
Current (mA)
Voltage (mV)
0.8
0.4
0.0
-20
-10
0
10
20
(a)
(b)
(c)
Signal (μV)
Time (ns)
0
500
90
60
30
10
5
20

Figure3

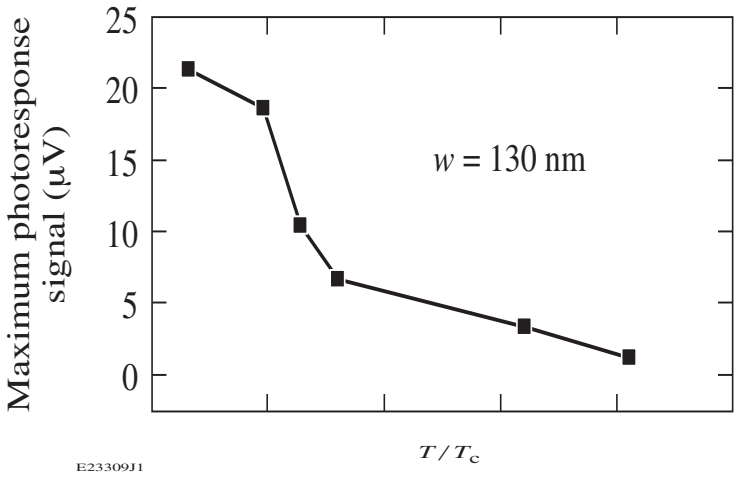
Maximum photoresponse signal (μV)
25
20
15
10
5
0
w = 130 nm
T / T_c
E23309J1

Figure 4

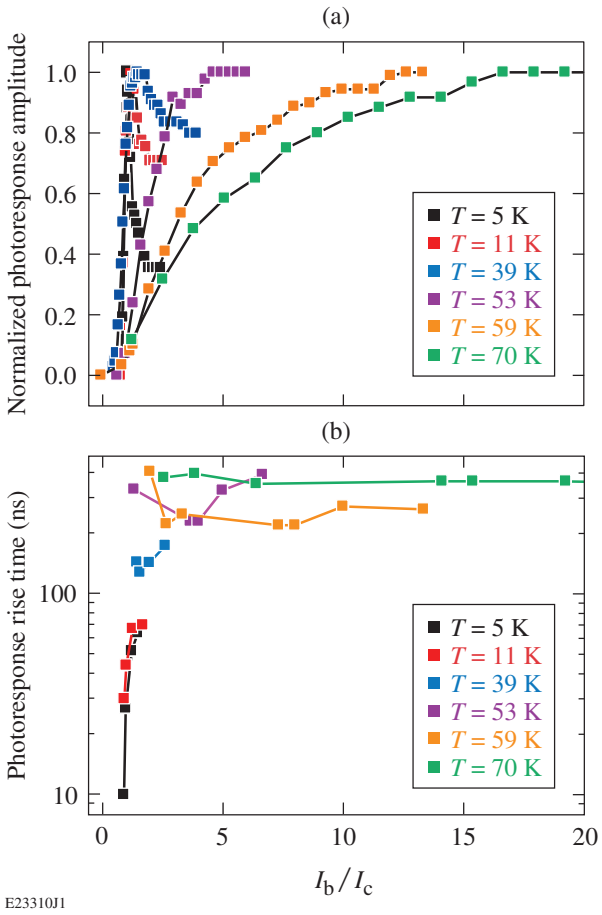
(a)
Normalized photoresponse amplitude
1.0
0.8
0.6
0.4
0.2
0.0
T = 5 K
T = 11 K
T = 39 K
T = 53 K
T = 59 K
T = 70 K
(b)
Photoresponse rise time (ns)
100
10
0
5
10
15
20
I_b / I_c
E23310J1

Figure 5